# Properties and Morphology of Supertoughened Polyamide 6 Hybrid Composites

**Yun Ding,[1,2] Guangxin Chen,[1,3] Jiangxuan Song,[1,3] Yunshu Gou,[1,3] Jianjun Shi,[1,3] Riguang Jin,[3] Qifang Li[1,3]**

[1]*Key Laboratory on Preparation and Processing of Novel Polymer Materials of Beijing, Beijing 100029, People's Republic of China*
[2]*College of Mechanical and Electrical Engineering, Beijing University of Chemical Technology, Beijing 100029, People's Republic of China*
[3]*College of Materials Science and Engineering, Beijing University of Chemical Technology, Beijing 100029, People's Republic of China*

Received 21 March 2011; accepted 1 December 2011
DOI 10.1002/app.36624
Published online in Wiley Online Library (wileyonlinelibrary.com).

**ABSTRACT:** In this study, supertoughened polyamide (PA) nanocomposites were prepared by the incorporation of epoxidized polyhedral oligomeric silsesquioxane (POSS) into the polyamide 6 (PA6)/methyl methacrylate–butadiene–styrene copolymer (MBS) blend via a melt-blending method. The effect of POSS on the rheological properties, mechanical properties, water uptake, and morphology of the hybrid PA6 nanocomposites was studied. The results show that under impact loading, the hybrid PA6 composites exhibited significant improvements in both the crack initiation energy and the crack propagation energy. This hybrid composite showed supertough behavior. Meanwhile, the tensile strength and the water absorption resistance was also improved with the addition of epoxidized POSS. The capillary and torque rheological results indicated that the epoxidized POSS, which acted as nanoscale ball bearings, significantly decreased the melt viscosity of the matrices and facilitated the melting process. Scanning electron microscopy (SEM) and transmission electron microscopy (TEM) were performed to study the microstructure–property relationships of the hybrid PA6 composites. The TEM results showed that the MBS particles were dispersed homogeneously in the PA6 matrix. The mean diameter of the MBS particles decreased, and the size distribution of the MBS particles narrowed down with the introduction of the epoxidized POSS and compatiblizer. The SEM micrographs indicated that the impact fracture surfaces of the PA composites showed morphological characteristics of supertough polymers because of the synergistic effect of the functionalized POSS and compatibilized MBS particles. © 2012 Wiley Periodicals, Inc. J Appl Polym Sci 000: 000–000, 2012

**Key words:** composites; morphology; polyamides

## INTRODUCTION

Polyamide 6 (PA6) has been widely used as a very important engineering plastic because of its advantages, which include a high strength, excellent wear resistance, and good chemical stability. However, PA6 has poor dimensional stability and notch toughness and a high moisture sorption; these restrict its more versatile application in the plastics and fiber industries.[1]

The blending of immiscible polymers is one of the most efficient ways to obtain polyamide (PA) materials with specific properties because blending can combine the solvent resistance, high stiffness, and strength of PA6 with the good toughness of other polymers with appropriate compatibilization.[2–5] One immiscible blend system that has attracted interest from both industry and academia is the blends of PA and some copolymers, such as acrylonitrile–butadiene–styrene (ABS), methyl methacrylate–butadiene–styrene copolymer (MBS or M), and styrene–ethylene/butadiene–styrene (SEBS) triblock copolymers. It is generally believed that the interfacial adhesion between the dispersed rubber particles and the polymer matrix plays an important role in toughening the matrix. Various compatibilizers have been extensively investigated to improve the interfacial adhesion.[2–7] In addition to the interfacial adhesion between the dispersed phase particles and the matrix (rubber particles), the dispersed phase particle size has been shown to be critical for improving the toughness of these blends.[8]

On the other hand, constituent binary PA nanocomposites have also been widely studied to pursue the generation of high-performance polymer-based

*Correspondence to:* Q. Li (qflee@mail.buct.edu.cn or echody@sohu.com).

Contract grant sponsor: Polymer Chemistry and Physics, Beijing Municipal Education Commission; contract grant number: XK100100640.
Contract grant sponsor: National Natural Science Foundation of China; contract grant number: 20974013.
Contract grant sponsor: Beijing Natural Science Foundation; contract grant number: 2072015.

nanocomposites with the combined advantages of nanometer materials and polymer matrices. Various nanoscale organic and inorganic materials, such as clays,[9,10] $CaCO_3$,[11] carbon nanotubes,[12] boehmite,[13] polyhedral oligomeric silsesquioxane (POSS or S),[14] and functionalized graphene,[15] have been tried to improve the multifunctional properties of polymer–matrix composites. The interfacial interactions between nanometer fillers and polymeric matrices play a very important role in the mechanical properties of the final polymer–matrix composites.

POSS-based nanocomposites are one kind of widely studied hybrid material. The general formula of POSS is $[RSiO_{3/2}]_n$. POSS consists of a central core that is around 1–3 nm surrounded by a different number of organic groups (R). The feasibility of controlling the arm number, length, and functionality makes POSS ideal for the preparation of nanocomposites.[16] Recently, POSS nanoparticles have been successfully dispersed or incorporated in various polymer matrices, such as EPOXY/POSS,[17,18] polyolefin/POSS,[19,20] polystyrene/POSS,[21,22] poly(methyl methacrylate)/POSS,[23,24] poly(ethylene terephthalate)/POSS,[25] and poly(lactic acid)/POSS,[26,27] to improve the mechanical properties, thermal stability, and rheological properties and to decrease the dielectric constant and flammability.[28,29] POSS can also be inserted into the PA matrix by different synthetic and melt-compounding methods. The versatility of the POSS organic substituents attached to each cage Si atom can improve compatibility with the polymer matrix and achieve property enhancements of PAs to some extent. Hybrid PA6 nanocomposites can be prepared with POSS with a reactive side group that is able to form a covalent link with the PA.[30] One study found that with increasing POSS content from 2 to 4 phr, the morphology of poly(2,6-dimethyl-1,4-phenylene oxide)/PA6 blends modified with epoxycyclohexyl POSS transformed from a droplet/matrix to a cocontinuous morphology. The poly(2,6-dimethyl-1,4-phenylene oxide)/PA6/POSS composites with a cocontinuous morphology had better mechanical properties than those with the droplet/matrix morphology.[31] In addition, polyamide 12/trisilanolphenyl–POSS (PA12/POSS) nanocomposites were prepared by a melt-compounding method. The addition of POSS enhanced the tensile strength and thermal stability of PA 12.[32]

Here, it is worth noting that no matter whether POSS or other rigid nanoparticles were incorporated into the PA matrix, the binary PA nanocomposites showed brittle behavior under impact conditions.[11,12] In the meantime, because of the low elastic modulus of rubber elastomers, PA/elastomer materials will decrease the stiffness and strength of the polymer matrix distinctly. The majority of commercial polymer blends possess a multiphase morphology, and satisfactory physical and mechanical properties are generally related to the presence of a finely dispersed phase and the resistance to gross phase segregation.[33] Therefore, a novel approach based on hybrid composites to prepare supertoughened PA6 nanocomposites (PA6/elastomer/POSS) is effective because they possess better properties than either of the constituent binary polymer composites (PA6/POSS or PA6/elastomer).

In this study, on the basis of our research work in the field of POSS synthesis and application,[22,34] an epoxidized POSS was synthesized and incorporated into the PA6/elastomer matrix with the aims of preparing supertoughened PA nanocomposites and improving other properties of the PA composites. The fracture toughness and mechanism of the nanocomposites were investigated with an instrumented impact tester. The load-time/displacement history of the specimen during the event of fracture was evaluated by an instrumented striker. The objective of this work was to develop a simple method with an instrumented Charpy impact testing machine to estimate the effects of POSS and other components on the impact energy of the nanocomposites. Furthermore, the effects of POSS on the rheological properties, tensile properties, water uptake, and morphology of the hybrid PA composites were also explored.

## EXPERIMENTAL

### Materials

The materials we used were as follows:

1. PA6 (UBE nylon 1013B, supplied by Japan UBE Nylon, Ltd., Tokyo, Japan).
2. MBS (Paraloid EXL2691A, supplied by Rohm & Hass Co., Philadelphia, Pennsylvania, United States). MBS had a core–shell structure, with the core made of a moderate crosslinking elastomer and the hard shell consisting of methyl methacrylate–styrene copolymers.
3. Diglycidyl ether of bisphenol A (DGEBA or D) epoxy resin (LER2050, supplied by LG Chem., Ltd., Seoul, Korea).
4. Epoxidized POSS. This was a dry white powder synthesized by our research group according to a method in the literature[35] (Fig. 1).

IR (KBr, $cm^{-1}$): 1109 (υ Si—O—Si); 780 (υ Si—C); 878, 1234 (υC—O—C of epoxy); 1330 (δ C—H of epoxy); 1604 (υ C=C); 1408, 1277 (δ C—H of vinyl), where υ represents the stretching mode and δ represents the bending mode. $^{29}$Si-NMR (ppm): −80.23 [$SiO_3C$ (vinyl)], −77.56 [$SiO_3C$ (epoxy)].

The IR and NMR results show that partial epoxidation of POSS was achieved from octavinyl silsesquioxane. The matrix-assisted laser desorption/ionization

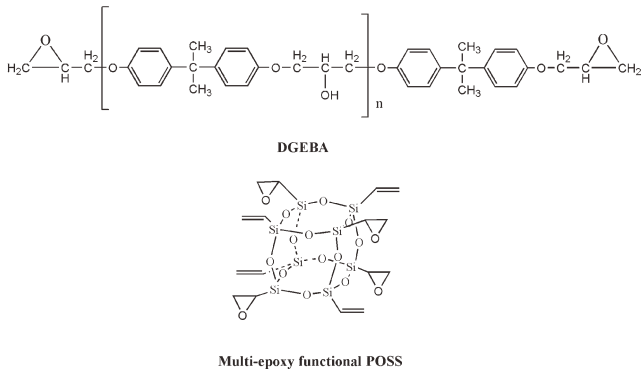


**Figure 1** Scheme of the molecular structure of the DGEBA and epoxidized POSS.

mass spectroscopy (Product + $Na^+$) values were as follows: 687.8 $m/z$ ($M_{di\text{-}epoxy}$ + $Na^+$, 24%), 703.8 $m/z$ ($M_{tri\text{-}epoxy}$ + $Na^+$, 81%), 719.8 $m/z$ ($M_{tetra\text{-}epoxy}$ + $Na^+$, 100%), 735.8 $m/z$ ($M_{penta\text{-}epoxy}$ + $Na^+$, 64%), and 751.8 $m/z$ ($M_{hexa\text{-}epoxy}$ + $Na^+$, 23%). M: the relative molecular mass of product. The matrix-assisted laser desorption/ionization mass spectroscopy analysis indicated that an average of four vinyls were epoxidized.

## Sample preparation

Before processing, PA6 was vacuum-dried for at least 10 h at 80°C, and the other components were vacuum-dried for 5 h at 40°C.

Before blending, the components of each blend, listed in Table I, were premixed in a 1.5-L sealed container for 15 min. Then, the premixed material was added to a Buss MKS30-F40 reciprocating single-screw laboratory kneader (Pratteln, Switzerland). The nanocomposites were performed with this Buss laboratory kneader. The screw diameters of the Buss laboratory kneader were 30 mm (the first stage) and 40 mm (the second stage). The extrusion temperatures of the Buss kneader were 200°C (hopper) and 210, 220, 230, and 240°C (die). The screw speed was 120 rpm, and the throughput was 8 kg/h. The blends were extruded as twin laces 2 mm in diameter; these were hauled into a quenching water trough before they were pelletized.

The dried compounds were molded to form impact specimens with an ARBURG 270S injection-molding machine (Lossburg, Germany). The barrel temperature profile was 210°C (hopper) to 240°C (nozzle), and the mold temperature was maintained at 40°C. The impact specimen size was 80 × 10 × 4 $mm^3$. Charpy impact tests were carried out on the notched specimens. The notches (depth = 2.0 mm, radius = 0.25 mm) were machined after injection molding. After specimen preparation was completed, the blends were conditioned at ambient temperature for at least 48 h before their properties were measured.

Five multiphase blend compositions were studied. Table I lists the weight ratio of each component in the formulation.

## Measurements and characterizations

### Torque rheological properties

The melt rheological characteristics of these hybrids were measured with a Haake torque rheometer (Haake Polylab System, Karlsruhe, Germany) with a 60-mL mixing chamber, and the torque was recorded for 6 min, typically, at 60 rpm and 245°C.

### Capillary rheometry

A RHEOGRAPH25 capillary rheometer by Goettfert Instruments (Buchen, Germany) was used to measure the apparent viscosity ($\eta_{ap}$) as a function of the shear rate at 245°C. The capillary rheometer had a capillary radius (R) of 0.5 mm and a length (L) of 40 mm (length-to-diameter ratio = 40) with a 90° degree entry angle. π: circular constant (about 3.14159). No end corrections were applied. $\eta_{ap}$ is the ratio of the apparent shear stress ($\tau_{ap}$) to $\gamma_{ap}$. With the dimensions of the capillary bore, the volumetric flow rate ($Q$) of the material through the capillary and the pressure differential ($\Delta P$) across the capillary ($\eta_{ap}$) was calculated by Eq. (1):

$$\eta_{ap} = \frac{\tau_{ap}}{\gamma_{ap}} = \frac{\pi \Delta P R^4}{8QL} \quad (1)$$

### Impact properties

The impact properties were studied with a Ceast 6957 pendulum-type instrumented Resil impact tester (Pianezza, Italy). The Charpy impact strength and the instantaneous impact curves were determined for the notched specimens according to ISO179 at an impact velocity speed of 2.9 m/s and at 23 ± 2°C and 50 ± 5% relative humidity. A minimum of five impact specimens were tested for each reported value. The load–time/displacement history of the specimen during the event of fracture was evaluated by an instrumented striker.

### Tensile properties

The tensile properties were measured with a SNAS testing machine from Shenzhen Sansi Co. (Shenzhen,

**TABLE I**
**Sample Codes and Compositions of the PA Blends**

| | Weight ratio | | | |
|---|---|---|---|---|
| Sample code | PA6 | MBS | DGEBA | POSS |
| PA | 100 | — | — | — |
| PA/M | 80 | 20 | — | — |
| PA/M/S | 80 | 20 | — | 1 |
| PA/M/D | 80 | 20 | 2 | — |
| PA/M/D/S | 80 | 20 | 2 | 1 |

China) according to ISO 527 at room temperature. A minimum of five impact specimens were tested for each reported value.

### Morphological observation

The impact fracture surface morphology of the blends was observed with a Cambridge Co. (Cambridge, United Kingdom) S-250 MK3 scanning electron microscope at a voltage of 20 kV with gold sputtering on the fractured surface.

The microstructural observation of the MBS particles was performed with a Philips EM400 transmission electron microscope (Eindhoven, Nederlands) at an accelerating voltage of 100 keV. Specimens about 80 nm thick were prepared for transmission electron microscopy (TEM) from the core region of the injection-molded tensile test pieces with a Reichert Ultracut ultramicrotome fitted with a diamond knife and then stained by exposure for 30 min to $O_SO_4$ vapors at ambient temperature.

The mean diameter ($D_{mean}$) and size distribution of the MBS particles were calculated from measurements of the TEM micrographs with Image-Pro Plus version 5.1 software from Media Cybernetics, Inc. (Silver Spring, Maryland, United States) $D_{mean}$ is defined as the average of line length connecting two outline points through the centroid at a 2° interval.

### Water uptake

The water uptake (WA; %) was calculated with Eq. (2):

$$WA(\%) = [(W_{wet} - W_{dry})/W_{dry}] \times 100\% \qquad (2)$$

where $W_{wet}$ and $W_{dry}$ are the wet weight and dried weight, respectively, of the composites. According to ASTM D 570-98, the conditioned specimens were immersed in (1) deionized water at room temperature for 24 h and (2) boiling distilled water for 2 h and were then removed quickly and blotted with filter paper to remove any excess water on the specimen surface. They were immediately weighed to obtain $W_{wet}$. $W_{dry}$ of the sample was measured after the sample was dried at 50°C for 24 h. The values obtained were the average of three readings.

## RESULTS AND DISCUSSION

### Rheology characteristics

The rheology behaviors of the blends reflected the mobility of the molecular chains and the interaction among the components. Figure 2 shows the equilibrium torque versus time for different formulations.

As compared with neat PA6, the equilibrium torque increased when MBS was added to the PA matrix. The equilibrium torque of the torque rheometer was closely related to the melt viscosity of the composites. The equilibrium torque of the PA/M/D blend increased sharply with the incorporation of DGEBA into the PA/M blend. This indicated there was a significant increase in the melt viscosity. This was attributed to the reaction of the epoxy groups with the end groups of PA6 at elevated temperatures (Fig. 3). However, the epoxy groups of both DGEBA and POSS reacted more preferentially to the amine end groups than to the carboxyl end groups, as reported.[31,36] There was a stronger chemical bonding between the DGEBA epoxy groups and the amine groups of matrix, and hydrogen bonds were readily generated between the hydroxyl groups on the DGEBA and the carbonyl groups on the poly (methyl methacrylate) shell of the MBS particles. This greatly increased the entanglement of the molecular chains and resulted in a higher melt strength and torque.[6,36] Therefore, DGEBA was an effective agent for enhancing the compatibility between the PA resin matrix and MBS and was helpful in breaking up the aggregation of MBS particles. When POSS was added to the PA/M matrix, the equilibrium torque decreased. In addition, with the incorporation of POSS into the matrix of PA/M/D, the equilibrium torque of PA/M/D/S decreased dramatically, too. This suggests that the addition of epoxy-functional POSS into the PA composites tended to cause a great decrease in the melt viscosity of the matrices and a significant improvement in the melt processing properties. The viscosities of the PA/M/D/S blend decreased compared with that of the PA/M/D system. This indicated that there was a weaker molecular interaction between the end groups of PA6 and the epoxy groups of POSS in comparison with DGEBA. As was known to us, functional POSS presents better compatibility with a polar polymer matrix.[30,31] However, the arm (R on the corner) length of POSS cage used in this study

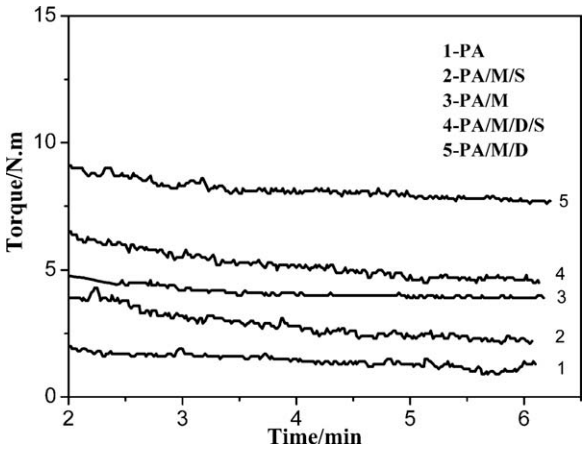


**Figure 2** Equilibrium torque versus time curves of different PA6 composites.

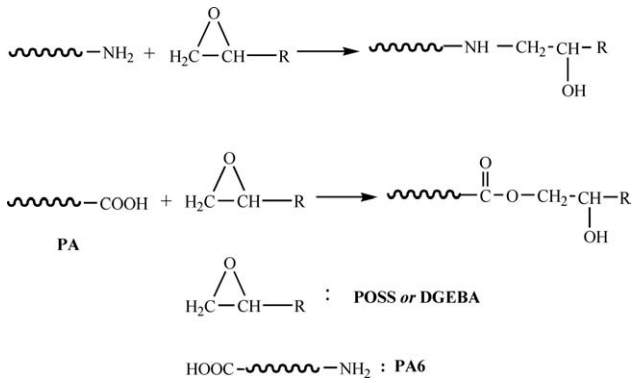


**Figure 3** Reaction between the end groups of the PA6 and DGEBA/POSS epoxy groups.

was short, and the epoxy end groups were adjacent the POSS cage backbone. It was thought that the segmental motion of the epoxy arm would be partly hindered by the steric hindrance of the POSS cage. Thus, the epoxidized POSS could behave as activated nanoscale ball bearings. The POSS at low loadings acted more like a nanoparticle plasticizer or flow aid[37] and facilitated the decrease in molecular entanglement of the matrices. This contributed to the further dispersion of MBS particles in the PA6 matrix during the melting period.

The rheological properties of the POSS-modified PA multiphase composites were further investigated by capillary rheological data, and the results are shown in Figure 4. Figure 4 displays the double logarithmic plots of log $\eta_{ap}$ versus log $\gamma_{ap}$ for all of the specimen melts at 245°C. As shown in Figure 4, all of the systems showed a typical shear-thinning behavior over the range of accessible shear rates. The PA6/M composite displayed a substantially higher $\eta_{ap}$ compared to pure PA6. The rheological behavior of the multiphase system was significantly influenced by the morphology, viscosity, and interfacial interaction of the two phases.[38] The level of PA6/M/DGEBA viscosity increased with the addition of DGEBA compatibilizer compared to PA6/M. This was possibly due to the improvement in the interfacial interaction between the PA and MBS components, which was related to the reaction between DGEBA and the end groups of PA6. This phenomena was examined in the Haake torque rheological test. It was clear that DGEBA had a considerable influence on the rheological behavior in the low-shear-rate region, whereas the incorporation of compatiblizer had no significant affect on the composite viscosity at a higher shear rate. A similar result was reported for PA6/ABS/EnBACO–MAH composites.[39] It could be seen that $\eta_{ap}$ of the PA/M/POSS composite with 1 wt % POSS loading was lower than that of the PA/M blend. Compared with the PA/M/DGEBA blend, the PA/M/DGEBA/POSS composite also exhibited a lower $\eta_{ap}$. This behavior was consistent with the results of the Haake torque rheological analysis. Results showing POSS leading to a viscosity reduction in other composites, such as poly(lactic acid), PPSU, and PP, at low POSS loadings have been reported in other publications.[26,40,41] POSS acted as an internal lubricator and effectively promoted flow. POSS probably led to the occurrence of disentanglement, interlayer slippage, and more free volume in the melt and, thus, resulted in the lower melt viscosity.[26]

## Impact properties

The instantaneous impact absorbed energy and load–time/displacement history under impact conditions was easily obtained from the novel instrumented impact tester. The values of maximum load, energy corresponding to maximum load, and total absorbed energy causing the fracture of the specimen were

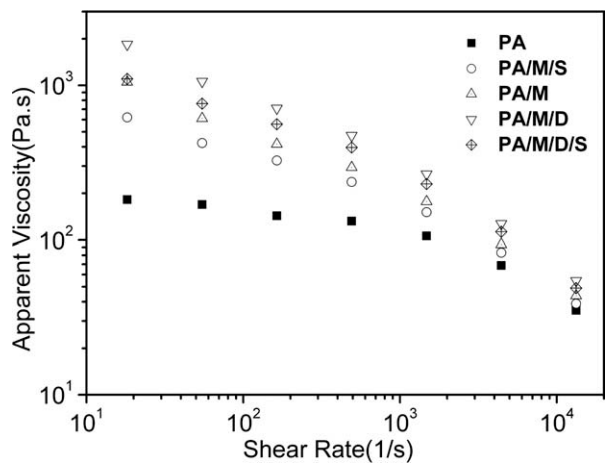


**Figure 4** Log–log plot of the $\eta_{ap}$ values of different composites.

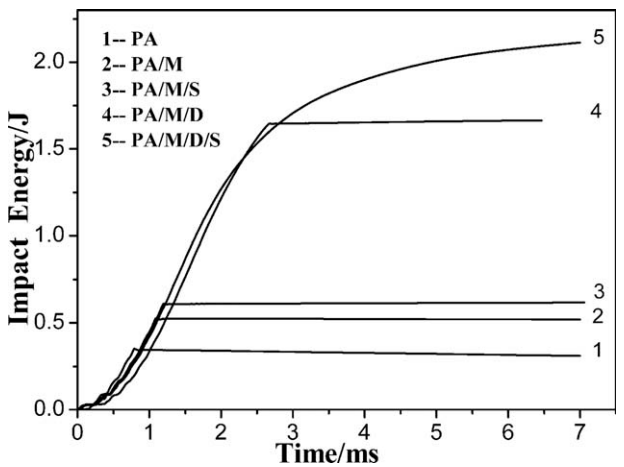


**Figure 5** Curves of instantaneous absorbed energy versus time for different materials.

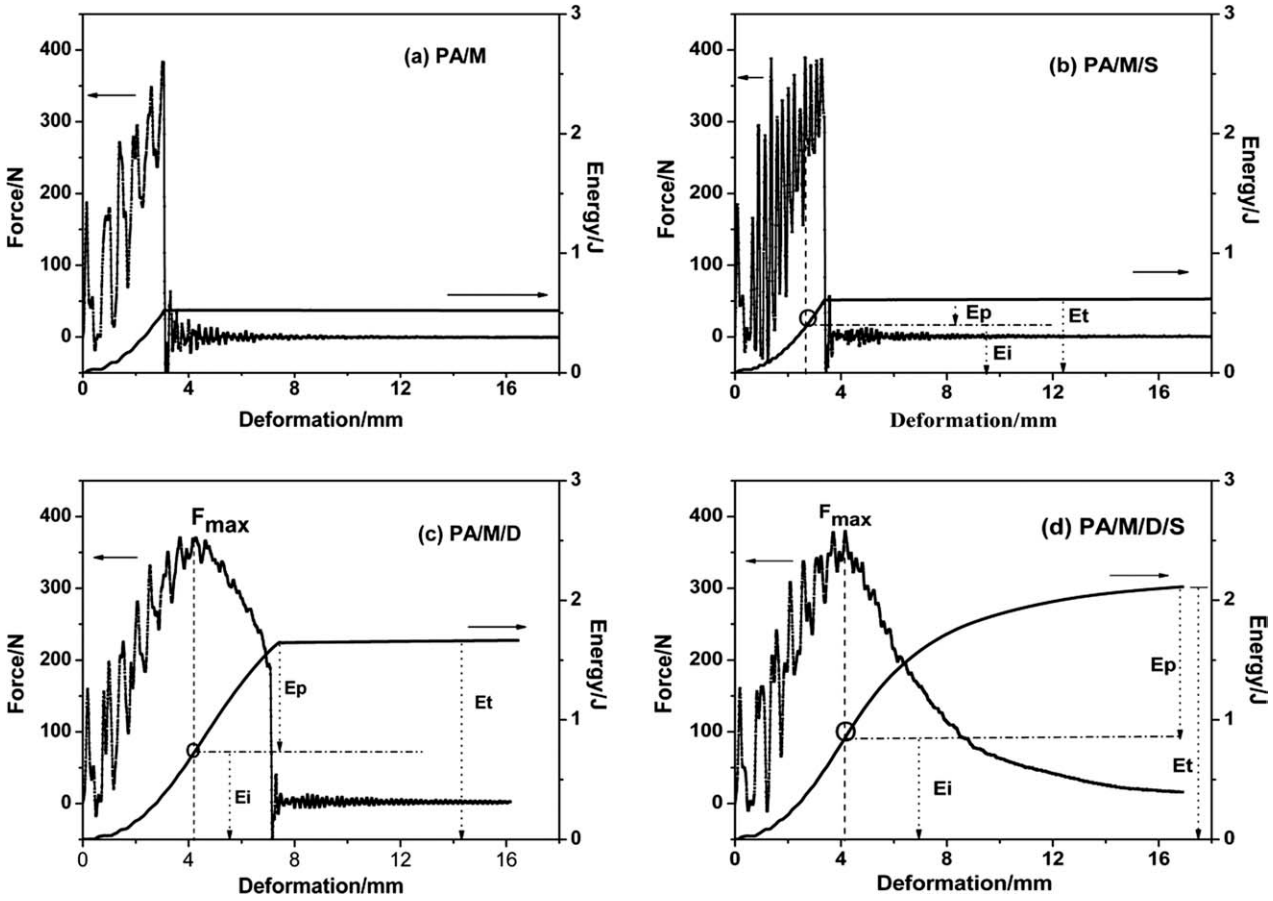


**Figure 6** Force and energy curves of different polymer systems as a function of deformation: (a) PA/M, (b) PA/M/S, (c) PA/M/D, and (d) PA/M/D/S.

estimated from the load–time/deformation signal. Figure 5 shows the instantaneous absorbed energy versus time for the materials at 23°C. The absorbed energy of the PA/M/S system was higher than that of the neat PA6 and PA/M blend. The absorbed energy of the PA/M/D/S system reached the maximum energy with the incorporation of functional POSS into the PA/M/D composite. The energy curve of the PA/M/D/S composite was a typical absorbed energy curve of a supertough material. The notched impact strength of the PA/M/D/S composite calculated according to the total impact absorbed energy reached a high value of 66 kJ/m$^2$. Thus, supertoughened PA composites containing a low concentration of elastomer were prepared via the addition of functional POSS.

According to the deformation behavior of the specimen, the total energy ($E_t$) generally could be divided into the crack initiation energy ($E_i$), which was the area under the load–displacement curve up to a maximum load point ($F_{max}$), and the crack-propagation energy ($E_p$), which was the area under the load–displacement curve from the maximum load point up to complete fracture.[42] Figure 6 shows the load–deformation curves of these composites. During the event of impact, a crack was initiated at the root of the notch, extended laterally, and reached the edges of the specimen when the maximum load was reached. The PA/M specimens still exhibited brittle fracture when the load dropped abruptly from the peak to zero. This implied that once crack was produced, the crack propagation of the PA/M system was very fast. In contrast to the PA/M system, the PA/M/S composite experienced some yield deformation after the maximum load peak; this led to an increased $E_p$ compared to the PA/M system. In comparison to the PA/M/D system, the PA/M/D/S blend fractured in a fully ductile manner, showing general yielding followed by a maximum load and a gradual load drop until the test ended. The deformation of the PA/M/D/S system was larger than that of the PA/M/D system after the maximum load was reached and so was its $E_p$ value.

The data from the instrumented impact tester was used to investigate the mechanism of toughening and to explore the function of POSS in these systems. Figure 7 shows visual bar plots comparing $E_i$ and $E_p$ for the different composites. It is generally known that PAs are notch-sensitive; hence, there was a very low $E_i$ and almost no $E_p$ for the prenotched specimen of neat PA. $E_i$ of the PA/M

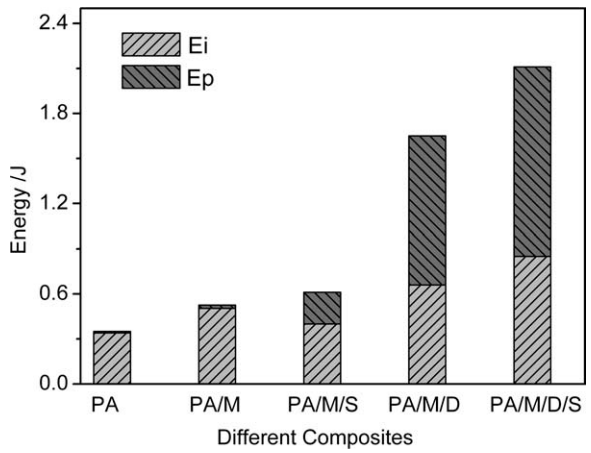


**Figure 7** Comparison of $E_i$ and $E_p$ for different polymer systems.

system increased with the incorporation of MBS into the PA matrix, but MBS brought only a marginal improvement in $E_p$. This was caused by a lack of good compatibility between MBS and the PA matrix. The PA/M/S system showed a minor increase in $E_i$ but a remarkable enhancement in $E_p$ in comparison with the PA6 and PA/M composite. This indicated that the POSS nanoparticles hindered crack propagation at the crack tip and were beneficial to the creation of large crazing; this was of great advantage to the enhancement of the energy absorption of the matrix. For the PA/M/D blend, the increases in both $E_i$ and $E_p$ were significant. We concluded that the compatibility of PA6 and MBS was promoted by the incorporation of DGEBA into the matrix. When the test specimen was under the same impact load, crack propagation could be prevented because of the improved bonding between PA6 and MBS. Then, more microcracks and shear bands were initiated. It is worth mentioning that the increases in both $E_i$ and $E_p$ for the PA/M/D/S system were most significant. First, the POSS nanoparticles themselves resulted in significant crack-tip blunting and led to an increase in the resistance to crack propagation. In addition, POSS, behaving as nanoscale ball bearings, facilitated the movement of the polymer matrix and helped to further segregate the aggregation of the MBS particles. Second, the uniform dispersion of compatibilized MBS particles further increased $E_i$ and $E_p$ of the PA composites. Thus, the PA composites were toughened by the synergistic effect of the hierarchical POSS nanoparticles and compatibilized MBS particles. The $E_t$ value for the PA/M/D/S reached the highest level.

### Tensile behavior

The tensile strength and elongation at break of the PA nanocomposites are given in Figure 8. Compared to the neat PA matrix, the tensile strength decreased a little after the addition of the MBS elastomer. This was partly due to the low strength of the elastomers and the poor combination of the PA6 and the shell of the MBS elastomers. For the PA/M/S composite, there was a small increase in the tensile strength after POSS was incorporated into the PA/M system. The addition of rigid nanoparticles improved the impact resistance of the PA6/elastomer without sacrificing its tensile properties. For the PA/M/D composite, the good combination of PA6 and MBS led to great increases in the tensile strength and elongation at break due to the addition of the compatibilizer (DGEBA). The tensile strength exhibited a maximum at the point where the POSS nanoparticles were introduced into the PA/M/D composite. Therefore, the results demonstrate a moderate increase in the tensile properties after the incorporation of both POSS and DGEBA into the PA/M blend, and meanwhile, the impact properties were improved significantly.

### Water uptake

Excess water sorption caused reduced mechanical properties and poor dimension stability in the PA composites; this implied the importance of the water absorption resistance properties. Figure 9 shows the water uptake (%) of different composites. Two kinds of water immersion methods were used. As shown in Figure 9, the water uptake of the neat PA relative to those of the other tested PA composites was higher, especially under boiling water conditions. It is known that the water absorption of PA is caused by the swelling of the amorphous phase with absorbed water. For the PA/M/S composite, functionalized POSS was well dispersed in the polymer matrix, and the presence of the nanocomposites led to a decrease in the water-diffusion rate because of

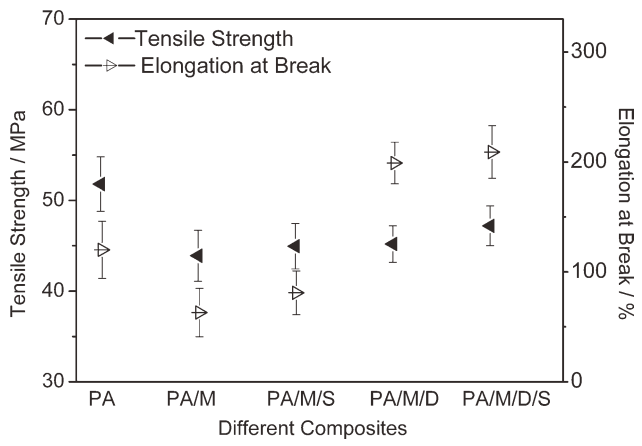


**Figure 8** Tensile strength and elongation at break of different PA6 composites.

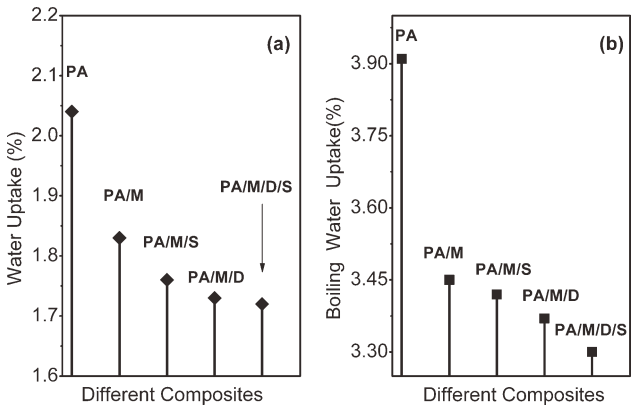


**Figure 9** Water uptake in the PA6 and PA6 composites: (a) normal and (b) boiling water uptake.

the barrier properties of the nano-POSS cage (because of their relatively hydrophobic core). In addition, DGEBA restrained the chain-segment mobility of the amorphous phase of PA because of the reaction between the epoxy group and the PA end groups. This caused a decrease in the water absorption in the PA/M/D composite. Thus, with the simultaneous introduction of both POSS and DGEBA into the PA/M blend, the water uptake of PA/M/D/S decreased obviously, especially the boiling water uptake.

### Morphological observations

Figure 10 shows low-magnification scanning electron microscopy (SEM) fractographs of the pure PA6 and its blends. The notch root is noted by an arrow. The impact fracture surfaces of the neat PA6 [Fig. 10(a)] and PA6/M binary composite [Fig. 10(b)] were similar and showed a typical brittle morphology, with hackles (occupying the majority of the fracture area) emanating radially from the primary crack initiation site (identified by a red circle). The SEM image of the PA/M/POSS blend [Fig. 10(c)] showed that the matrix surfaces exhibited more corrugated lamellar structures. When more cavitations were initiated, the polymer blends could absorb more impact energy. For the PA/M/D composite, ductile tearing on adjacent planes was obvious, and this contributed to energy absorption in this material [Fig. 10(d)]. Furthermore, parallel bands were visible on the notched impact fracture surface. These bands have been observed in many ductile polymeric materials and are not only formed by the propagation of the main crack but are also associated with secondary cracks, which initiate at separate nuclei and propagate radially outward.[12] A representative SEM micrograph for PA6/M/DGEBA/POSS is shown in Figure 10(e). It was surprising that predominant ductile tearing behavior and fine parallel bands were found on the entire fracture surface of this nanocomposite. This was displayed in the mechanical properties as a dramatic increase in the impact toughness, and the matrix resin was transferred from ductile material into a supertoughened material.

To further elucidate the effect of POSS on the toughness properties of the hybrid composites, TEM was employed to study the microstructures of the materials, as shown in Figure 11. Figure 12 shows the calculated particle $D_{mean}$ and the size distribution of the MBS particles. Serious aggregation of the MBS particles was observed, as shown in Figure 11(a).

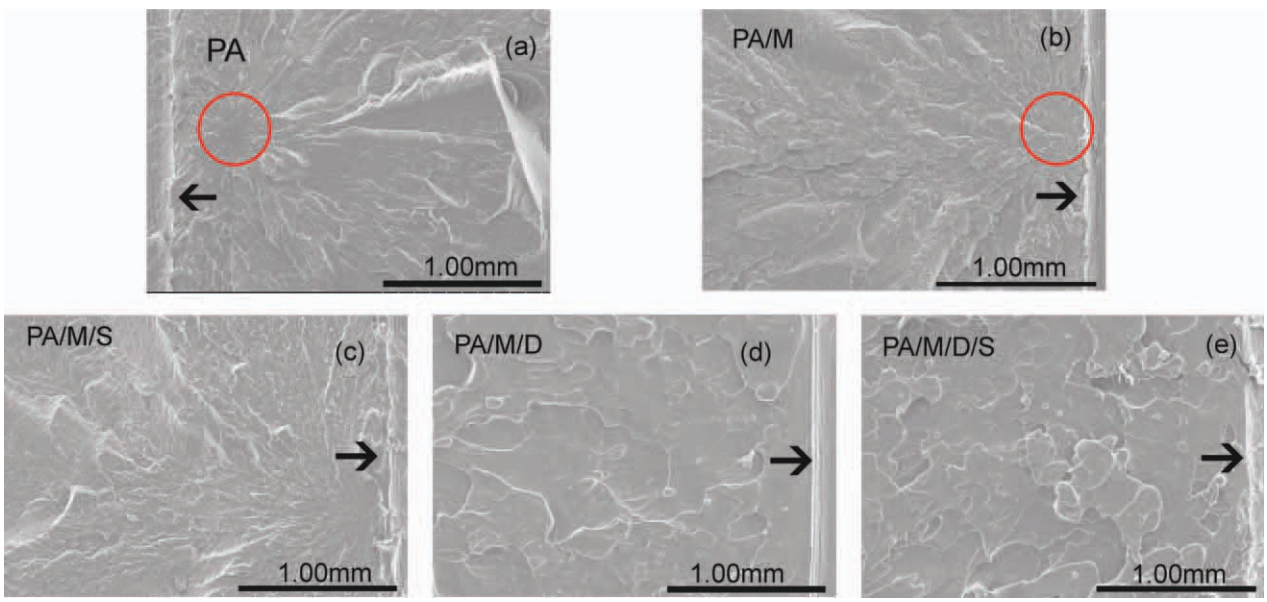


**Figure 10** SEM micrographs of the impact–fracture surfaces of the pure PA6 and its blends. [Color figure can be viewed in the online issue, which is available at wileyonlinelibrary.com.]

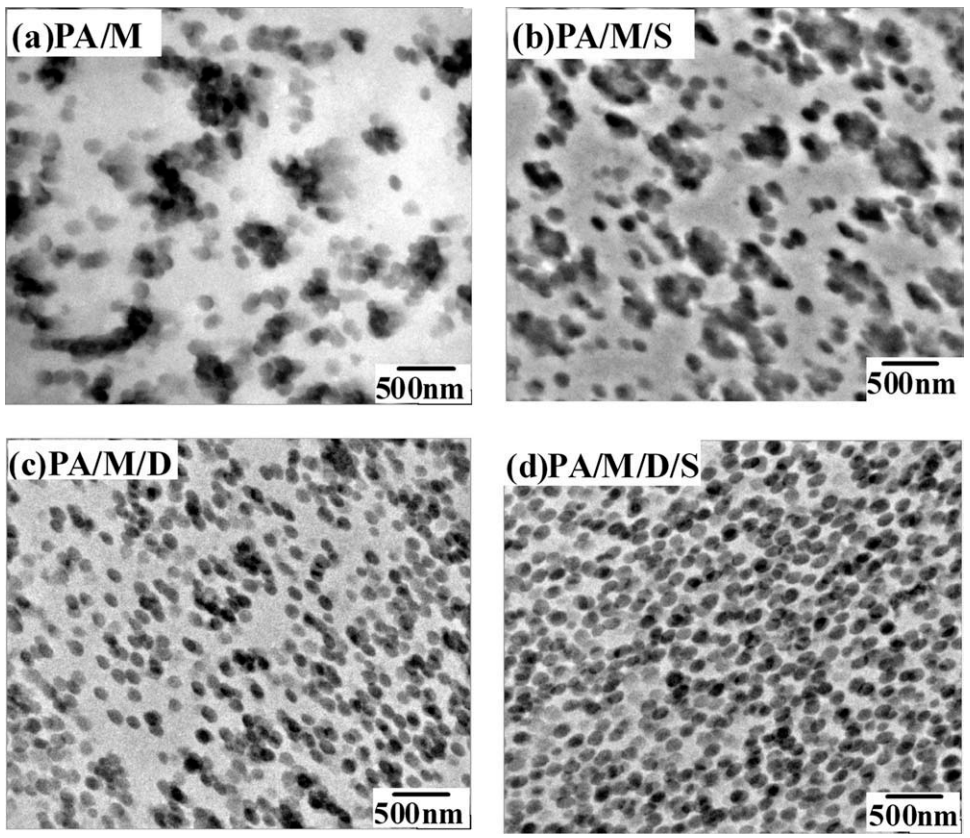


**Figure 11** TEM images of (a) PA/M, (b) PA/M/S, (c) PA/M/D, and (d) PA/M/D/S blends ($OsO_4$ stained).

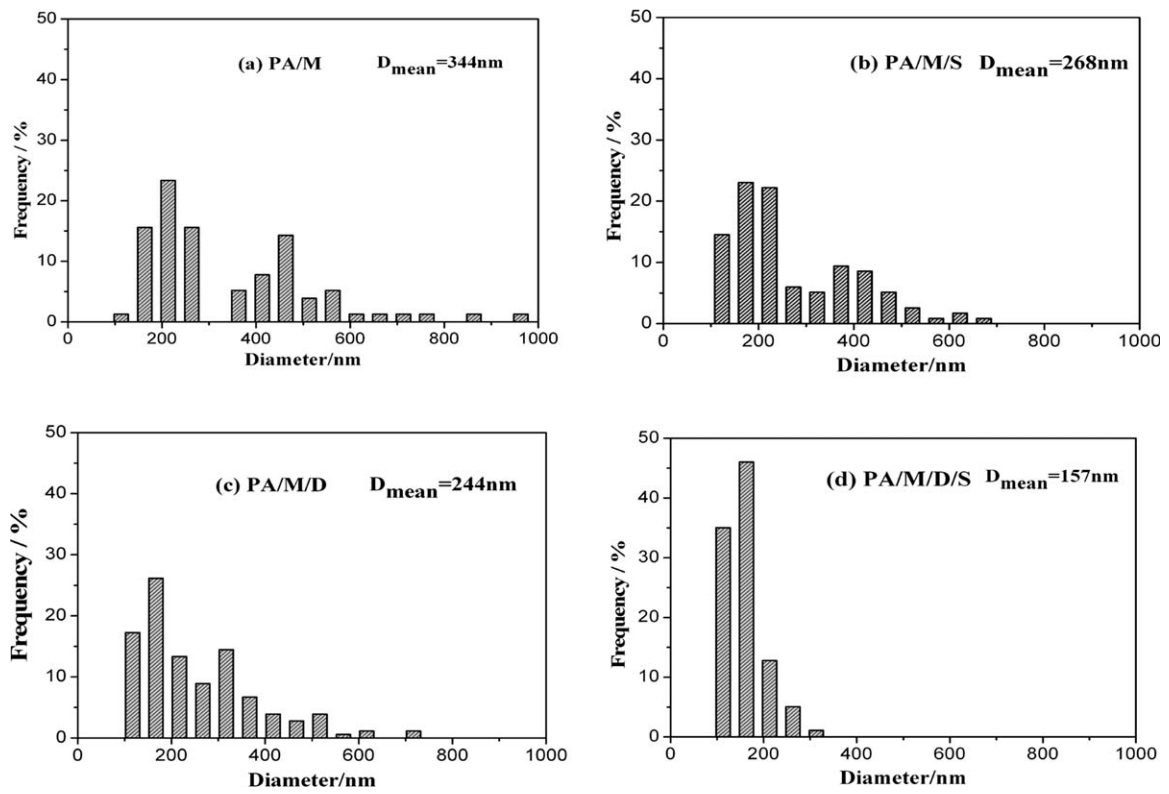


**Figure 12** $D_{mean}$ and size distribution values of the MBS particles for different PA composites: (a) PA/M, (b) PA/M/S, (c) PA/M/D, and (d) PA/M/D/S.

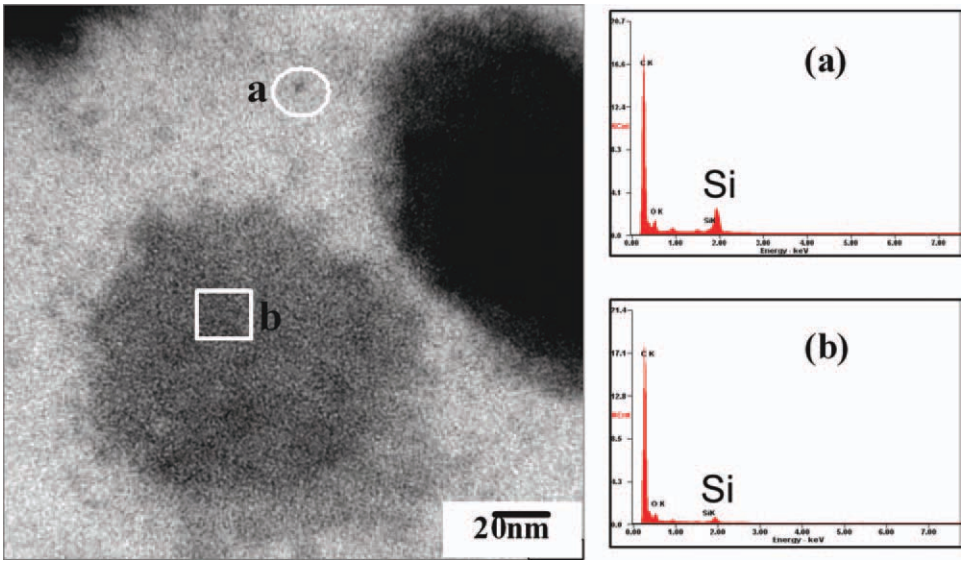


**Figure 13** EDAX of the PA/M/D/S composites (a) at the interzone region between the MBS particles and PA6 matrix and (b) on the surface of the MBS particles. [Color figure can be viewed in the online issue, which is available at wileyonlinelibrary.com.]

Without any efficient compatibilizers incorporated into the PA6/M blend, $D_{mean}$ was very large, and the size distribution of the MBS particles was uneven, as shown in Figure 12(a). Figure 11(b) shows that the aggregation of MBS particles decreased with the incorporation of POSS into the PA/M composite. Figure 12(b) demonstrates that the size distribution of the MBS particles was narrow for the PA/M/S composite. We concluded from Figure 11(c) that the aggregation of MBS particles was reduced with the incorporation of DGEBA into the PA/M system. It is also revealed in Figure 12(c) that $D_{mean}$ of the MBS particles for the PA/M/D composite decreased from 344 to 244 nm. For the PA/M/D/S system, it is shown in Figure 11(d) that the dispersed domains were well dispersed throughout the PA6 matrix. $D_{mean}$ of the MBS particles decreased to 157 nm, as shown in Figure 12(d). We concluded that the introduction of both POSS and DGEBA into the PA6/M blend dramatically improved the dispersion of MBS particles and narrowed the size distribution. It was suggested by Wu[8] that the toughness of rubber-modified thermoplastics increased as the ligament size was reduced. The interparticle distance or ligament size can be reduced either by increasing the rubber concentration or by decreasing the rubber particle size. The increase in the impact strength of PA/M/D/S was attributed mainly to the decreases in the MBS particle size and interparticle distance due to the incorporation of POSS and DGEBA. Figure 13 summarizes the energy spectrum analysis (EDAX) of the PA/M/D/S composite. It is seen that the silicon-rich region in the PA/M/D/S composite was located at the interface region around the MBS particles; this implies that most of the POSS molecules were dispersed in these regions. The incorporation of POSS nanoparticles further reduced the MBS mean particles size and resulted in the uniform dispersion of MBS particles. As a result, many more microcracks and shear bands were produced at the edge of MBS particles when the sample was under impact load. Meanwhile, both POSS and compatibilized MBS particles were capable of preventing crack-tip propagation. This enhanced the absorbed impact energy of the composites before specimen fracture happened. Figure 14 shows the presumed dispersion mechanism of hierarchical particles

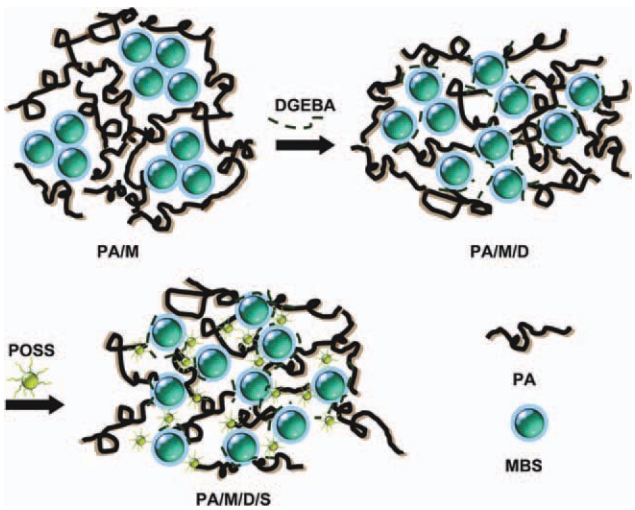


**Figure 14** Presumed dispersion mechanism of the hierarchical particles in the PA matrix. [Color figure can be viewed in the online issue, which is available at wileyonlinelibrary.com.]

in the PA matrix. At first, the MBS particles were big and aggregated in the PA matrix. Then, with the incorporation of DGEBA into the PA6/M composite, the improved compatibility and the increased melt viscosity facilitated the dispersion of MBS particles and led to a decrease in the MBS particle $D_{mean}$ and a narrow size distribution. Finally, with the introduction of POSS into the PA/M/D composite, a uniform dispersion of MBS elastomers was present.

## CONCLUSIONS

In this study, a novel epoxidized POSS was incorporated into a PA6/M blend to prepare high-performance hybrid composites. $E_i$ and the crack propagation energy ($E_p$) of the PA6/M/DGEBA/POSS composite increased significantly under impact loading. TEM micrographs showed that the compatibilized MBS particles dispersed homogeneously in the PA6 matrix for this composite. $D_{mean}$ of the MBS particles decreased, and the size distribution of the MBS particles narrowed; these changes were attributed to the introduction of the epoxy POSS and DGEBA. SEM micrographs of this hybrid nanocomposite showed morphological characteristics of supertoughened materials. Predominant ductile tearing behavior and fine parallel bands were found on the entire fracture surface of this nanocomposite. With the addition of low contents of POSS into the PA6 composites, the hierarchical structure of the POSS nanoparticles and compatibilized MBS particles exhibited synergistic toughening effects. Thus, supertough composites were prepared. Furthermore, the rheological measurement showed that POSS acted as nanoscale ball bearings and significantly decreased the viscosity and equilibrium torque of the hybrid materials. The tensile properties increased slightly after the incorporation of both POSS and DGEBA into the PA6/M blend. The water absorption of the PA6/M/DGEBA/POSS composite was reduced. This means that the mechanical properties and dimensional stability would be less sensitive to short-term fluctuations under normal environmental conditions than those of unfilled PA6. Therefore, it is believed that this novel approach to hybrid nanocomposites was effective for preparing a new high-performance and functional PA material.

### References


1. Li, D. L.; Liu, Q.; Yu, L. G.; Li, X. H.; Zhang, Z. J. Appl Surf Sci 2009, 255, 7871.
2. Gonzalez, I.; Eguiazabal, J. I.; Nazabal, J. Compos Sci Technol 2006, 66, 1833.
3. Harada, T.; Carome, E.; Kudva, R.; Keskkula, H.; Paul, D. R. Polymer 1999, 40, 3957.
4. Arostegui, A.; Nazabal, J. Polymer 2003, 44, 239.
5. Chiang, C. R.; Chang, F. C. J Appl Polym Sci 1996, 61, 2411.
6. Wang, X. D.; Li, H. Q. J Appl Polym Sci 2000, 77, 24.
7. Araujo, E. M.; Hage, J. R. E.; Carvalho, A. J. F. J Mater Sci 2004, 39, 1173.
8. Wu, S. Polymer 1985, 26, 1855.
9. Bureau, M. N.; Denault, J.; Cole, K. C.; Enright, G. D. Polym Eng Sci 2002, 42, 1897.
10. Okamoto, M.; Morita, S.; Kotaka, T. Polymer 2001, 42, 2685.
11. Wilbrink, M. W. L.; Argon, A. S.; Cohen, R. E.; Weinberg, M. Polymer 2001, 42, 10155.
12. Dasari, A.; Yu, Z. Z.; Mai, Y. W. Polymer 2009, 50, 4112.
13. Zdilek, C.; Kazimierczak, K.; David, B.; Stephen, J. Polymer 2004, 45, 5207.
14. Kuo, S. W.; Chang, F. C. Prog Polym Sci 2011, 36, 1649.
15. Rafiq, R.; Cai, D. Y.; Jin, J.; Song, M. Carbon 2010, 48, 4309.
16. Lee, L. H.; Chen, W. C. Polymer 2005, 46, 2163.
17. Lee, A.; Lichtenhan, J. D. Macromolecules 1998, 31, 4970.
18. Kourkoutsaki, T. H.; Logakis, E.; Kroutilová, I.; Matějka, L. J Appl Polym Sci 2009, 113, 2569.
19. Fu, B. X.; Yang, L.; Somani, R. H.; Zong, S. X.; Hsiao, B. S.; Phillips, S. J Polym Sci Part B: Polym Phys 2001, 39, 2727.
20. Zheng, L.; Farris, R. J.; Coughlin, E. B. Macromolecules 2001, 34, 8034.
21. Yang, B. H.; Xu, H. Y.; Wang, J. F.; Gang, S. Y.; Li, C. J Appl Polym Sci 2007, 106, 320.
22. Song, X. Y.; Geng, H. P.; Li, Q. F. Polymer 2006, 47, 3049.
23. Feng, Y.; Jia, Y.; Xu, H. Y. J Appl Polym Sci 2009, 111, 2684.
24. Kopesky, E. T.; Haddad, T. S.; McKinley, G. H.; Cohen, R. E. Polymer 2005, 46, 4743.
25. Yoon, K. H.; Polk, M. B.; Park, J. H.; Min, B. G.; Schiraldi, D. A. Polym Int 2005, 54, 47.
26. Wang, R. Y.; Wang, S. F.; Zhang, Y. J Appl Polym Sci 2009, 113, 3095.
27. Lee, J. H.; Jeong, Y. G. J Appl Polym Sci 2010, 115, 1039.
28. Huang, X. Y.; Xie, L. Y.; Jiang, P. K.; Wang, G. L.; Yin, Y. Eur Polym J 2009, 45, 2172
29. Bourbigot, S.; Duquesne, S.; Jama, C. Macromol Symp 2006, 233, 180
30. Ricco, L.;Russo. S. Monticellia, O.; Bordoa, A.; Belluccia, F. Polymer 2005, 46, 6810.
31. Li, B.; Zhang, Y.; Wang, S.; Ji, J. L. Eur Polym J 2009, 45, 2202.
32. Wan, C. Y.; Zhao, F.; Bao, X. J.; Kandasubramanian, B.; Duggan, M. J Polym Sci Part B: Polym Phys 2009, 47, 121.
33. Wilkinson, A. N.; Clemens, M. L.; Harding, V. M. Polymer 2004, 45, 5239.
34. Song, J. X.; Chen, G. X.; Wu, G.; Cai, C. H.; Liu, P. G.; Li, Q. F. Polym Adv Technol 2010, 22, 206.
35. Zhang, J. Q.; Li, Q. F. Fine Chem 2007, 24, 17.
36. Wang, K. Y.; Chen, Y. M.; Zhang, Y. Polymer 2009, 50, 1483.
37. Phillips, S. H.; Haddad, T. S.; Tomczak, S. J. Curr Opin Solid State Mater Sci 2004, 8, 21.
38. Jeon, H. S.; Nakatani, A. I.; Han, C. C.; Colby, R. H. Macromolecules 2000, 33, 9732.
39. Mojarrad, A.; Jahani, Y.; Barikani, M. J Appl Polym Sci 2011, 120, 2173.
40. Jones, P. J.; Cook, R. D.; McWright, C. N.; Nalty, R. J.; Choudhary, V.; Morgan, S. E. J Appl Polym Sci 2011, 121, 2945.
41. Zhou, Z.; Zhang, Y.; Zhang, Y.; Yin, N. J Polym Sci Part B: Polym Phys 2008, 46, 526.
42. Viswanathan, U. K.; Singh, R. N.; Basak, C. B.; Anantharaman, S.; Sahoo, K. C. J Nucl Mater 2006, 350, 310.